Romanian Reports in Physics **71**, 412 (2019)

NONLINEAR CONICAL DIFFRACTION IN SUPERHONEYCOMB LATTICE INDUCED IN A PHOTOREFRACTIVE CRYSTAL

YIQING TIAN[1], HUA ZHONG[2,3,4,*], MILIVOJ R. BELIĆ[5], YANPENG ZHANG[3], FULI LI[2], YIQI ZHANG[3,4,**]

[1]School of Physics and Optoeletronic Engineering, Xidian University, Xi'an 710071, China
[2]Department of Applied Physics, School of Science, Xi'an Jiaotong University, Xi'an 710049, China
[3]Key Laboratory for Physical Electronics and Devices of the Ministry of Education & Shaanxi Key Lab of Information Photonic Technique, School of Electronic Science and Engineering, Xi'an Jiaotong University, Xi'an 710049, China
[4]Guangdong Xi'an Jiaotong University Academy, Foshan 528300, China
[5]Science Program, Texas A&M University at Qatar, P. O. Box 23874 Doha, Qatar
[*]zhonghua@stu.xjtu.edu.cn
[**]zhangyiqi@mail.xjtu.edu.cn

Received July 30, 2019

Abstract. We report nonlinear conical diffraction in the superhoneycomb lattice, which is an edge-centered honeycomb lattice, induced in a photorefractive crystal. This system is of special interest, as it represents a hybrid fermionic – bosonic physical system. When nonlinearity is imposed, conical diffraction from a fermionic Dirac cone will change from circular diffraction rings, formed by small hexagons, into a triangular arrangement of hexagons. But from the bosonic Dirac cone, conical diffraction changes into elliptic diffraction rings of different inner symmetries, with the outer ring intensity damped.

Key words: Superhoneycomb lattice, nonlinear conical diffraction, photorefractive crystal.

1. INTRODUCTION

Photorefractive (PR) crystals are extensively used in nonlinear optics in the past few decades, due to the tunability of their refractive index change through an external bias electric field. One of the most charming properties of PR crystals is that optical lattices or waveguide arrays can be induced in a quite simple manner; such a property is quite useful in investigating discrete solitons [1–5], quantum analogies [6, 7], and related topological topics [8–11]. Indeed, the honeycomb and Lieb lattices have stirred a lot of interest in topological photonics [12–17]. In previous research, it has been proven that the superhoneycomb lattice combines the honeycomb lattice and the Lieb lattice and displays the properties of both. It contains two different kinds of Dirac cones, which demonstrates that the superhoneycomb lattice is a hybrid fermionic – bosonic system [18, 19]. The first two bands, as well as the last two bands in the superhoneycomb lattice intersect at a set of diabolic Dirac points at six

corners of the first Brillouin zone, forming Dirac cones in the band structure. Such Dirac cones are of the pseudospin-1/2 type. Whereas the Dirac point located at the intersection of the flat band corresponds to the pseudospin-1 type.

Thus, the key feature related to the appearance of conical diffraction is the existence of Dirac cones in the band structure. However, not all photonic lattices support conical diffraction – only those with Dirac cones that are driven by the symmetry of the lattice structure. In the vicinity of a Dirac cone, the dispersion is nearly linear, which indicates that the first-order derivative of the energy band is constant and the second-order derivative is zero. This means that the transverse radius of the beam that excites the Dirac cone state will linearly grow with the propagation distance and gives rise to a circular conical diffraction. Until now, the topic has been widely investigated in honeycomb lattice [20], Lieb lattice [21], and edge-centered square lattice [8, 22–24], to name a few. It is worth mentioning that Dirac cones are associated with different physical pseudospin systems, which can be substantiated through the mediated vortex generation, indicated in the formation process of conical diffraction [19, 25, 26].

In the superhoneycomb lattice, conical diffraction [19] and the line states [11] were reported previously, but only in the linear domain. In this paper, we are interested in what will happen when the nonlinearity is introduced into this hybrid system. Will the conical diffraction be substantially changed? Are there new phenomena in comparison with the nonlinear conical diffraction already observed in honeycomb and Lieb lattices? Thus, here we will investigate nonlinear conical diffraction in the superhoneycomb lattice based on the continuous model, which is more accurate than the tight-binding method. To excite the Dirac cone state effectively and avoid mathematical complexity along the way, we will use the method developed in Ref. [24].

2. SUPERHONEYCOMB LATTICE AND ITS BAND STRUCTURE

In an SBN photorefractive crystal, the dynamical behavior of a light beam can be described by the Schrödinger-like paraxial wave equation of the form:

$$i\frac{\partial\psi(x,y,z)}{\partial z} = -\frac{1}{2k_0}\left(\frac{\partial^2}{\partial x^2}+\frac{\partial^2}{\partial y^2}\right)\psi(x,y,z) - \frac{k_0\Delta n(x,y,z)}{n_0}\psi(x,y,z), \quad (1)$$

where x, y are the transverse spatial coordinates and z is the longitudinal propagation distance. Here, $\psi(x,y,z)$ is the slowly-varying envelope of the light beam during propagation, and $k_0 = 2n_0\pi/\lambda_0$ is the wave number, with the wavelength chosen as $\lambda_0 = 532\,\mathrm{nm}$, and $n_0 = 2.35$ is the ambient refractive index of the SBN crystal. Further, Δn is the refractive index change due to light, which, according to the PR

effect, is defined as:

$$\Delta n(x,y,z) = -\frac{1}{2}{n_0}^3 \gamma_{33} E_0 \frac{1}{1+I(x,y)+|\psi(x,y,z)|^2}, \tag{2}$$

where the bias field is $E_0 = 1\,\mathrm{kV/cm}$, the electro-optic coefficient $\gamma_{33} = 280\,\mathrm{pm/V}$, and $I(x,y)$ is the light intensity in the crystal that builds the lattice. Here, this intensity is arranged in a pattern that will induce a superhoneycomb lattice in the SBN crystal through

$$I(x,y) = \left| \sum_{m,n} a \exp\left(-\frac{(x-x_{m,n})^2 + (y-y_{m,n})^2}{w^2} \right) \right|^2, \tag{3}$$

where a represents the beam amplitude, $(x_{m,n}, y_{m,n})$ are the lattice sites, with (m,n) being integers, and w determines the beam width. For the distance between two nearest-neighbor (NN) lattice sites we take $d = 30\,\mu\mathrm{m}$, and for the width $w = 0.72\,\mu\mathrm{m}$.

We show the superhoneycomb lattice induced in the SBN photorefractive crystal in Fig. 1(a). The corresponding far-field diffraction pattern is displayed in Fig. 1(b), in which the first Brillouin zone (a hexagon) is clearly shown with high-symmetric points $\mathbf{K}$ and $\mathbf{K}'$ in the corners and the $\mathbf{\Gamma}$ point in the center. One finds that there is no difference between the Brillouin zones of the superhoneycomb lattice and the honeycomb lattice [27]; the difference is in the number of sites in the unit cell: honeycomb lattice has 2 and the superhoneycomb lattice has 5. Thus, the superhoneycomb lattice is formed by inserting another site in-between each NN pair of sites of the honeycomb lattice. The band structure of the superhoneycomb lattice is shown in Fig. 1(c). Usually, such band structures are reported using the tight-binding method [19]. However, the band structure obtained directly, based on the continuum model is more realistic, because the tight-binding method utilizes high-level approximations (*e.g.*, only the NN hopping is considered). The band calculation proceeds as follows.

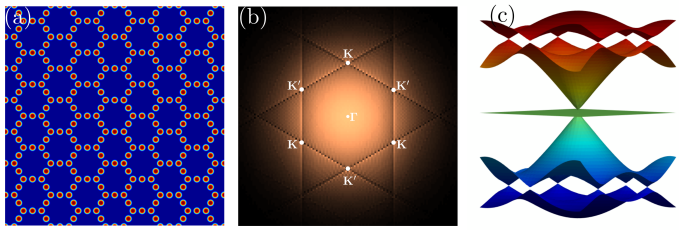

Fig. 1 – (a) The geometry of the superhoneycomb lattice. (b) Far-field diffraction pattern with high symmetric points of the first Brillouin zone. (c) Band structure.

For mathematical convenience, we transform Eq. (1) into a dimensionless equation by replacing x, y, and z with xr_0, yr_0, and zL_z with $L_z = k_0 r_0^2$ being

the Rayleigh range. Here, r_0 connects with the typical width of the incident beam. As a result, one obtains:

$$i\frac{\partial\psi(x,y,z)}{\partial z} = -\frac{1}{2}\left(\frac{\partial^2}{\partial x^2}+\frac{\partial^2}{\partial y^2}\right)\psi(x,y,z) - \frac{{k_0}^2{r_0}^2\Delta n(x,y)}{n_0}\psi(x,y,z). \quad (4)$$

To calculate the band structure based on the continuum model [24, 28, 29], we first rotate the frame from (x,y) into (X,Y) through the relation $X = x\cos(\theta) - y\sin(\theta)$, $Y = x\sin(\theta) + y\cos(\theta)$ and $Z = z$, with $\theta = \pi/6$. Then, we transform the lattice into the frame (x',y') through the relation $X = x' + y'\cos(\varphi)$, $Y = y'\sin(\varphi)$ and $Z = z'$, with $\varphi = \pi/3$. After these transformations, Eq. (4) reaches the form:

$$i\frac{\partial\psi(x,y,z)}{\partial z} = -\frac{2}{3}\left(\frac{\partial^2}{\partial x^2}+\frac{\partial^2}{\partial y^2}-\frac{\partial^2}{\partial x\partial y}\right)\psi(x,y,z) - \frac{{k_0}^2{r_0}^2\Delta n(x,y)}{n_0}\psi(x,y,z), \quad (5)$$

which is the starting point of our analysis. In Eq. (5), we use again (x,y,z) as the coordinates, rather than (x',y',z'), for notational simplicity. In the band calculation, we neglect the nonlinear term $|\psi(x,y,z)|^2$ in Δn and look for the solution of the form $\psi(x,y,z) = u(x,y)\exp(i\beta z)$, with β being the propagation constant. So, one obtains:

$$\beta u(x,y) = \frac{2}{3}\left(\frac{\partial^2}{\partial x^2}+\frac{\partial^2}{\partial y^2}-\frac{\partial^2}{\partial x\partial y}\right)u(x,y) + \frac{{k_0}^2{r_0}^2\Delta n(x,y)}{n_0}u(x,y), \quad (6)$$

which represents an eigenvalue problem for β. Equation (6) can be solved by the plane-wave expansion method, to obtain the corresponding band structure, as shown in Fig. 1(c).

There are 5 sites in the unit cell and 5 bands in the band structure. We label the five bands in Fig. 1(c) as $\beta_1 \sim \beta_5$ from top to bottom, which include a flat band β_3 in the middle of the band structure. In the first two bands β_1 and β_2 and the last two bands β_4 and β_5, there are six Dirac points that reside at the corners of the first Brillouin zone. These Dirac points generate six Dirac cones that are visible in the band structure shown in Fig. 1(c). Since these Dirac cones are associated with the fermionic pseudospin system, we define them as Type-F Dirac cones.

At the intersection of the β_2 and β_4 bands, in-between which the flat band β_3 is situated, one can notice another kind of Dirac cone at the Γ point, which is related to the bosonic pseudospin system, and therefore we define it as Type-B Dirac cone. Clearly, Type-F and Type-B Dirac cones are corresponding to the pseudospin-1/2 and pseudospin-1 systems [18, 19], respectively. It is well known that the first-order derivatives $(d\beta/dk_x, d\beta/dk_y)$ of the band structure correspond to the components of the velocity of the states during propagation, and the second-order derivatives $(d^2\beta/dk_x^2, d^2\beta/dk_y^2)$ are the dispersions. The incident beam that excites the flat band will remain unchanged during propagation, and the beams that excite the Dirac cone

states will exhibit conical diffraction [19].

3. NONLINEAR CONICAL DIFFRACTION

Since there are two kinds of Dirac cones in the superhoneycomb lattice, it is reasonable to investigate the conical diffraction separately for the two kinds. We would like to note first that the bias field of $E_0 = 1\,\mathrm{kV/cm}$ will cause the beam to undergo self-focusing effect during propagation. Therefore, we will not consider the self-defocusing case in this work. Also, during propagation, the intensity $|\psi(x, y, z)|^2$ will build up, even if it started as small relative to $1 + I(x, y)$. Thus, after a while, the refractive index change Δn will develop into a saturable nonlinearity, and the conical diffraction will change from linear to nonlinear. This is the change in the conical diffraction we are looking for during beam propagation in the crystal.

The parameter we use to monitor the transition from linear to nonlinear conical diffraction is the power of the incident beam, $P = \iint |\psi(x, y, z = 0)|^2 dxdy$. For small P, the diffraction stays linear for long; as P increases, the transition to nonlinear diffraction becomes more rapid. For high P, no conical diffraction is observed. For the preparation of the incident beam, we use the Dirac cone states based on the method developed in Ref. [24], and then multiply them with a Gaussian beam.

3.1. TYPE-F DIRAC CONE

As concerns the Type-F Dirac cones, we consider first those between the β_1 and β_2 bands (labeled as D_{12}), and then between the β_4 and β_5 bands (labeled as D_{45}).

In the linear case, the incident beam should exhibit perfect conical diffraction during propagation, and the beam intensity distributions at selected normalized distances are drawn in Fig. 2(a1)-(a3). One finds that the conical diffraction indeed appears during propagation. The input beam is a solid circle at the initial place, with the input power $P = 1$ [Fig. 2(a1)], and it spreads linearly in radial directions during propagation, to form a ring-like structure of constant thickness [30], as shown in Figs. 2(a2) and 2(a3). When the power of the incident beam P is increased, the influence of nonlinearity becomes more obvious. In Fig. 2(b1), the power of the incident beam is $P \approx 4.94$. During nonlinear propagation, the beam also exhibits conical diffraction [Fig. 2(b2)], however, after a long distance the conical diffraction does not show a circular ring but a triangular profile, as displayed in Fig. 2(b3). Apparently, such a change is due to self-focusing nonlinearity. Further increasing the power of the incident beam to $P \approx 8.78$, as in Fig. 2(c1), the triangular conical diffraction becomes more pronounced [Figs. 2(c2) and 2(c3)]. More numerical simulations indicate that conical diffraction will disappear if the power of the incident beam is too large. Then,

the incident beam will just spread uniformly.

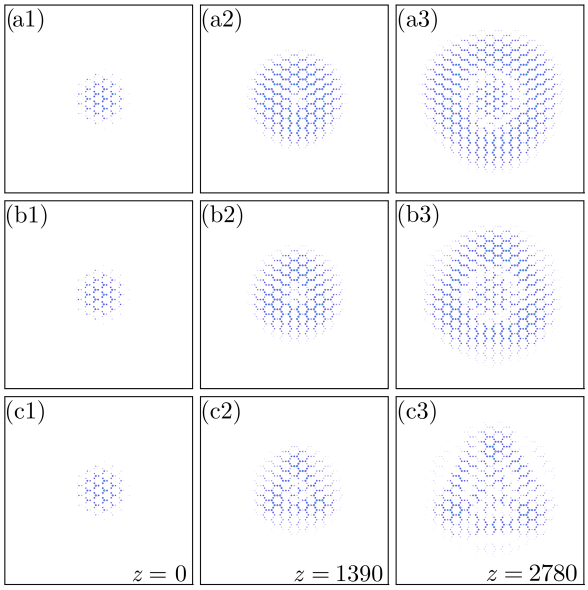

Fig. 2 – (a) Linear conical diffraction of the incident beam exciting the Dirac cone state between β_1 and β_2 bands. The incident beam power is 1. (b) Nonlinear conical diffraction with the incident power of 4.94. (c) Same as (b), but for the power 8.78. The panels are shown in the window $-139 \leq x \leq 139$, $-139 \leq y \leq 139$. The propagation distance is shown in the right-bottom corner of each panel.

Taking the same procedure, we study the nonlinear conical diffraction due to the D_{45} Dirac cones, and the results are shown in Fig. 3. In Figs. 3(a1)-3(a3), the linear conical diffraction is displayed, which corresponds to that in Figs. 2(a1)-2(a3). One finds that the radius of the conical diffraction ring in Fig. 3(a3) is a bit bigger than that in Fig. 2(a3). This means that the velocity $(d\beta/dk_x, d\beta/dk_y)$ around D_{45} is slightly bigger than that around D_{12}, even though they are seemingly the same. Incidentally, the band structure in Fig. 1(c) is quite similar to the one obtained by the tight-binding method [19]. However, the band structure obtained by the continuum model is not completely symmetric about the flat band β_3, which is also not completely flat. When nonlinearity is considered, similar to that in Fig. 2, the circular conical diffraction changes into a triangular conical diffraction.

From the nonlinear conical diffractions exhibited in Figs. 2 and 3, one finds that the nonlinearity can affect the conical diffraction from Type-F Dirac cones greatly, and it can result in the triangular diffraction patterns that deviate significantly from linear circular patterns.

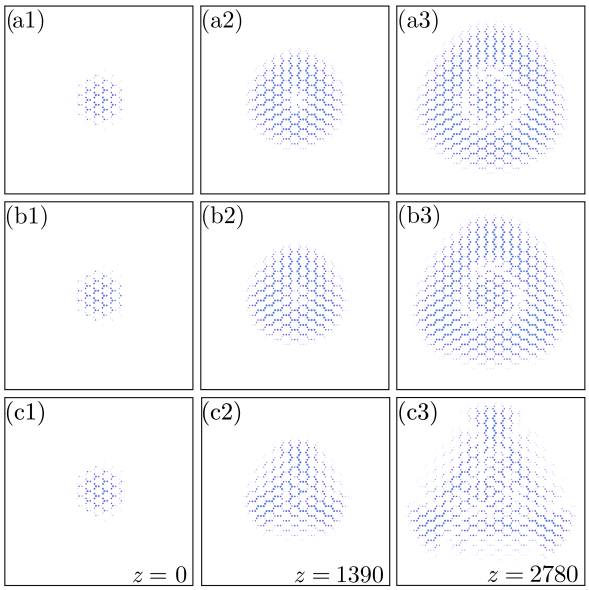

Fig. 3 – Figure setup is as Fig. 2, but for the Dirac cone state between β_4 and β_5 bands. The powers of the incident beam in (b) and (c) are 3.83 and 15.33, respectively.

3.2. TYPE-B DIRAC CONE

In this subsection, we explore the nonlinear conical diffraction from the Type-B Dirac cone [31]. The Dirac cone at $\mathbf{\Gamma}$ point is of pseudospin-1 type, which is bosonic-like, and therefore fundamentally different from the fermionic-like Dirac cones at $\mathbf{K}$ and $\mathbf{K}'$ points. Here, we will be concerned with the following questions: Is the nonlinear conical diffraction the same as that investigated above and displays triangular patterns? Since there is a flat band that cuts through the Type-B Dirac cone, are the nonlinear conical diffractions the same when the Dirac cone states are excited separately above and below the flat band? Having these questions in mind, we investigate the nonlinear conical diffraction from the Type-B Dirac cone, utilizing the same approach as used before.

We first show the results associated with the Type-B Dirac cone above the flat band, as in Fig. 4. In Figs. 4(a1)-4(a3), the linear conical diffraction is displayed. One finds that the phenomenon of the linear conical diffraction is quite similar in both Type-B and Type-F Dirac cones, except for the expansion speed. This is quite easy to understand. According to the band structure in Fig. 1(c), one finds that the first-order derivative of the Type-B Dirac cone is bigger than that of the Type-F Dirac cone. When the nonlinearity is considered, as shown in Fig. 4(b1)-4(b3), where $P \approx 22.79$, the conical diffraction still shows a circular ring, but the intensity along the ring edge obviously decreases [Fig. 4(b3)]. Also, the intensity inside the

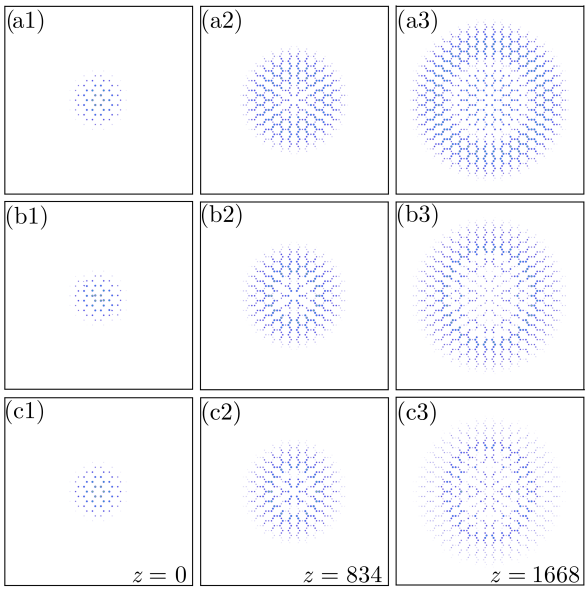

Fig. 4 – Figure setup is as Fig. 2, but for Dirac cone state between β_2 and β_3 bands. The powers of the incident beam in (b) and (c) are 22.79 and 29.77, respectively.

ring [Fig. 4(a3)] also decreases, due to nonlinearity. Further increasing the incident beam power to $P \approx 29.77$, the circular conical diffraction changes into an elliptic conical diffraction, as displayed in Figs. 4(c1)-4(c3). In Fig. 4(c3), the major axis of the elliptic ring is along the y axis. This is different from the nonlinear conical diffraction from the Type-F Dirac cones, where the triangular patterns are observed.

The results for the case when the Type-B Dirac cone state below the flat band is excited are shown in Fig. 5. Figure 5(a) displays the linear conical diffraction, which is quite similar to that in Fig. 4(a), because the absolute values of both $(d\beta/dk_x, d\beta/dk_y)$ and $(d^2\beta/dk_x^2, d^2\beta/dk_y^2)$ of the Dirac cone do not change above or below the flat band. When the nonlinearity is included, with the increasing incident beam power, the circular conical diffraction also changes into elliptic conical diffraction, as shown in Figs. 5(b1)-5(b3) and 5(c1)-5(c3). However, the major axis of the elliptic diffraction ring is now along the x axis, which is orthogonal to that shown in Fig. 4. Hence, one finds that not only the nonlinear conical diffractions from Type-F and Type-B Dirac cones are different, but also those from the Type-B Dirac cone above and below the flat band are different.

Obviously, nonlinearity brings more interesting results in the superhoneycomb lattice than in other lattices, and the hybrid superhoneycomb lattice exhibits enormous potential and possibilities for controlling light behavior.

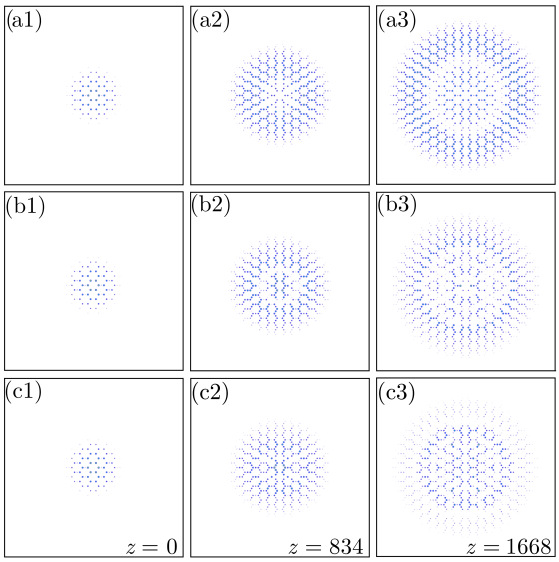

Fig. 5 – Figure setup is as Fig. 4, but for Dirac cone state between β_3 and β_4 bands. The powers of the incident beam in (b) and (c) are 30.97 and 44.6, respectively.

4. CONCLUSION

In conclusion, we have investigated conical diffraction in the superhoneycomb lattice, based on the continuous model. We display the nonlinear conical diffraction from Dirac cones at points $\mathbf{K}$ and $\mathbf{K}'$, as well as from the cone at $\mathbf{\Gamma}$ point. At $\mathbf{K}$ and $\mathbf{K}'$ points, the nonlinear conical diffraction exhibits triangular patterns, while at the $\mathbf{\Gamma}$ point, the nonlinear conical diffraction displays elliptic patterns. Based on our results, one finds that the nonlinearity indeed affects the conical diffraction substantially, and that the role is different in fermionic and bosonic Dirac cones. Our results may have potential applications in wavefront shaping and modulation.

Acknowledgements. This work was supported by the Fundamental Research Funds for the Central Universities (xzy012019038, xzy022019076), and Natural Science Foundation of Guangdong province (2018A0303130057). Work in Qatar was supported by the NPRP 11S-1126-170033 from the Qatar National Research Fund.

REFERENCES

1. J. W. Fleischer, M. Segev, N. K. Efremidis, D. N. Christodoulides, Nature **422**, 147–150 (2003).
2. N. K. Efremidis, S. Sears, D. N. Christodoulides, J. W. Fleischer, M. Segev, Phys. Rev. E **66**, 046602 (2002).
3. J. W. Fleischer, T. Carmon, M. Segev, N. K. Efremidis, D. N. Christodoulides, Phys. Rev. Lett. **90**, 023902 (2003).

4. H. Martin, E. D. Eugenieva, Z. Chen, D. N. Christodoulides, Phys. Rev. Lett. **92**, 123902 (2004).
5. J. W. Fleischer, G. Bartal, O. Cohen, O. Manela, M. Segev, J. Hudock, D. N. Christodoulides, Phys. Rev. Lett. **92**, 123904 (2004).
6. H. Trompeter, W. Krolikowski, D. N. Neshev, A. S. Desyatnikov, A. A. Sukhorukov, Y. S. Kivshar, T. Pertsch, U. Peschel, F. Lederer, Phys. Rev. Lett. **96**, 053903 (2006).
7. Y. Sun, D. Leykam, S. Nenni, D. Song, H. Chen, Y. D. Chong, Z. Chen, Phys. Rev. Lett. **121**, 033904 (2018).
8. D. Song, V. Paltoglou, S. Liu, Y. Zhu, D. Gallardo, L. Tang, J. Xu, M. Ablowitz, N. K. Efremidis, Z. Chen, Nat. Commun. **6**, 6272 (2015).
9. S. Xia, Y. Hu, D. Song, Y. Zong, L. Tang, Z. Chen, Opt. Lett. **41**, 1435–1438 (2016).
10. Y. Zong, S. Xia, L. Tang, D. Song, Y. Hu, Y. Pei, J. Su, Y. Li, Z. Chen, Opt. Express **24**, 8877–8885 (2016).
11. W. Yan, D. Song, S. Xia, L. Tang, Y. Q. Zhang, J. Xu, Z. Chen, in *Conference on Lasers and Electro-Optics*, p. FW3D.3 (Optical Society of America, 2019).
12. M. Kohmoto, Y. Hasegawa, Phys. Rev. B **76**, 205402 (2007).
13. O. Bahat-Treidel, O. Peleg, M. Grobman, N. Shapira, M. Segev, T. Pereg-Barnea, Phys. Rev. Lett. **104**, 063901 (2010).
14. M. C. Rechtsman, Y. Plotnik, J. M. Zeuner, D. Song, Z. Chen, A. Szameit, M. Segev, Phys. Rev. Lett. **111**, 103901 (2013).
15. V. Apaja, M. Hyrkäs, M. Manninen, Phys. Rev. A **82**, 041402 (2010).
16. N. Goldman, D. F. Urban, D. Bercioux, Phys. Rev. A **83**, 063601 (2011).
17. R. A. Vicencio, C. Cantillano, L. Morales-Inostroza, B. Real, C. Mejía-Cortés, S. Weimann, A. Szameit, M. I. Molina, Phys. Rev. Lett. **114**, 245503 (2015).
18. Z. Lan, N. Goldman, P. Öhberg, Phys. Rev. B **85**, 155451 (2012).
19. H. Zhong, Y. Q. Zhang, Y. Zhu, D. Zhang, C. B. Li, Y. P. Zhang, F. L. Li, M. R. Belić, M. Xiao, Ann. Phys. (Berlin) **529**(3), 1600258 (2017).
20. H. Leblond, B. A. Malomed, D. Mihalache, Phys. Rev. A **83**, 063825 (2011).
21. Y. Q. Zhang, X. Liu, M. Belić, W. P. Zhong, C. B. Li, H. X. Chen, Y. P. Zhang, Rom. Rep. Phys. **68**, 230–240 (2016).
22. T. Jacqmin, I. Carusotto, I. Sagnes, M. Abbarchi, D. D. Solnyshkov, G. Malpuech, E. Galopin, A. Lemaître, J. Bloch, A. Amo, Phys. Rev. Lett. **112**, 116402 (2014).
23. D. Song, S. Liu, V. Paltoglou, D. Gallardo, L. Tang, J. Zhao, J. Xu, N. K. Efremidis, Z. Chen, 2D Mater. **2**, 034007 (2015).
24. H. Zhong, R. Wang, M. R. Belić, Y. P. Zhang, Y. Q. Zhang, Opt. Express **27**(5), 6300–6309 (2019).
25. D. Leykam, O. Bahat-Treidel, A. S. Desyatnikov, Phys. Rev. A **86**, 031805 (2012).
26. F. Diebel, D. Leykam, S. Kroesen, C. Denz, A. S. Desyatnikov, Phys. Rev. Lett. **116**, 183902 (2016).
27. D. Zhang, Y. Q. Zhang, Z. Y. Zhang, N. Ahmed, Y. P. Zhang, F. L. Li, M. R. Belić, M. Xiao, Annalen der Physik **529**(9), 1700149 (2017).
28. Y. Plotnik, M. C. Rechtsman, D. Song, M. Heinrich, J. M. Zeuner, *et al.*, Nat. Mater. **13**, 57–62 (2014).
29. Y. V. Kartashov, D. V. Skryabin, Optica **3**(11), 1228–1236 (2016).
30. M. Berry, M. Jeffrey, Prog. Opt. **50**, 13–50 (2007).
31. D. Leykam, A. S. Desyatnikov, Adv. Phys. X **1**, 101–113 (2016).